


# Singularity-Enhanced Terahertz Detection in High-Mobility Field-Effect Transistors

M. Khayronin,<sup>1</sup> A. Petrov,<sup>1</sup> A.E. Kazantsev,<sup>2</sup> E.I. Nikulin,<sup>2</sup> and D.A. Bandurin<sup>3,1,\*</sup>

<sup>1</sup>Laboratory of 2d Materials for Optoelectronics, Moscow Institute of Physics and Technology, Dolgoprudny 141700, Russia

<sup>2</sup>Physics Department, M.V. Lomonosov Moscow State University, Moscow, Russia

<sup>3</sup>Department of Physics, Massachusetts Institute of Technology, Cambridge, Massachusetts 02139, USA

 (Received 16 March 2020; revised manuscript received 14 May 2020; accepted 1 June 2020; published 30 June 2020)

Detectors of high-frequency radiation based on high-electron-mobility transistors benefit from low noise, room-temperature operation, and the possibility to perform radiation spectroscopy using gate-tunable plasmon resonance. Despite successful proof-of-concept demonstrations, the responsivity of transistor-based detectors of terahertz radiation, at present, remains fairly poor. To resolve this problem, we propose a class of devices supporting singular plasmon modes, i.e., modes with strong electric fields near keen electrodes. A large plasmon-enhanced electric field results in amplified nonlinearities, and thus efficient ac-to-dc conversion. We analyse subterahertz detectors based on a two-dimensional electron system in the Corbino geometry as a prototypical and exactly solvable model, and show that the responsivity scales as  $1/r_0^2$  with the radius of the inner contact  $r_0$ . This enables responsivities exceeding 10 kV/W at subterahertz frequencies for nanometer-scale contacts readily accessible by modern nanofabrication techniques.

DOI: [10.1103/PhysRevApplied.13.064072](https://doi.org/10.1103/PhysRevApplied.13.064072)

## I. INTRODUCTION

Excitation of plasmons in radiation detectors provides a convenient tool to enhance absorption and thereby increase sensitivity [1–3]. Such enhancement in the visible and infrared ranges is easily achieved by the integration of metal nano-objects and photosensitive semiconductors [4]. This technique, however, cannot be extended to terahertz (THz) frequencies due to the high density of electrons in metals. This extension can be achieved with plasmons bound to the semiconductors themselves [5–7]. Apart from low carrier density, observation of plasmon resonance in the THz range requires long electron momentum relaxation time  $\tau_p$ , such that the quality factor,  $Q = \omega\tau_p$ , exceeds unity ( $\omega$  is the plasmon frequency). Such long relaxation times are favorably achieved in III-V heterostructures [8] and encapsulated graphene [9,10].

The conceptual scheme of plasmon-enhanced THz detector based on a two-dimensional electron system (2DES) was put forward in Ref. [11], and realized decades later with GaAs-based heterostructures [5–7,12] and graphene [10]. Such detectors consist of a field-effect transistor (FET) with a 2D channel and parallel source and drain contacts. THz radiation impinging on an antenna connected between source and gate creates an alternating

electric potential in the channel. Rectification by transistor nonlinearities results in a dc photovoltage between source and drain. The performance of this scheme was scarcely analyzed critically, and most experimental work on transistor-based THz detectors simply copied this proposal [13–15]. Still, it is apparent that such a detector structure is almost symmetric, while structural asymmetry is the key requirement to achieve photovoltage at zero bias.

In this paper, we show that the responsivity of transistor-based THz detectors can be greatly enhanced in structures supporting highly asymmetric THz plasmon modes with singular electric fields at the contacts. Such strong fields are generally formed near keen, or thin, electrodes. Importantly, these modes are associated with oscillations of 2D electrons, and not electrons in metal contacts [16]. This makes a conceptual difference with photodetectors enhanced by the plasmonic “lightning-rod” effect [17], allowing the resonance to move towards THz frequencies. The combined geometric and plasmonic field enhancement results in strong nonlinear rectification, especially for nonlinearities localized near the contacts [18,19].

We consider plasmon-assisted THz rectification in a gated 2DES in the Corbino disc geometry (see Fig. 1) as a prototypical and exactly solvable model system. We show that detector responsivity diverges as the radius of inner contact  $r_0$  tends to 0 according to  $r_0^{-2}$ , and is limited

\*bandurin@mit.edu

by the nonlocality of rectification mechanisms. Comparing the responsivity of FET-based detectors with parallel and concentric source and drain, we find that the latter exceeds the former by an order of magnitude already for  $R_0/r_0 = 30$ .

## II. DEVICE STRUCTURE AND MODEL

The combined geometric-plasmonic enhancement of detector responsivity is most clearly seen via an example of a 2DES transistor in the Corbino geometry (Fig. 1). High-frequency radiation impinging on the antenna connected to source and gate results in an alternating voltage,  $V_a \cos(\omega t)$ . Combined with fixed gate bias  $V_0$ , they form the time-dependent gate voltage

$$V_g(t) = V_0 + V_a \cos(\omega t). \quad (1)$$

Rectification of this voltage by various nonlinearities in the 2DES results in a dc photovoltage,  $\Delta V$ , read out between source and drain. For computational simplicity, we develop a theory of both linear response and rectification within the hydrodynamic approximation. The latter has recently been proven to hold at elevated temperatures in high-quality graphene devices [20–22]. We further argue that geometric and plasmonic enhancement holds for other rectification mechanisms and other transport regimes as well.

Electron motion in an axially symmetric Corbino device is governed by Euler's equation for the drift velocity  $u$ ,

$$\frac{\partial u}{\partial t} + u \frac{\partial u}{\partial r} + \frac{u}{\tau_p} = \frac{e}{m} \frac{\partial \varphi}{\partial r}, \quad (2)$$

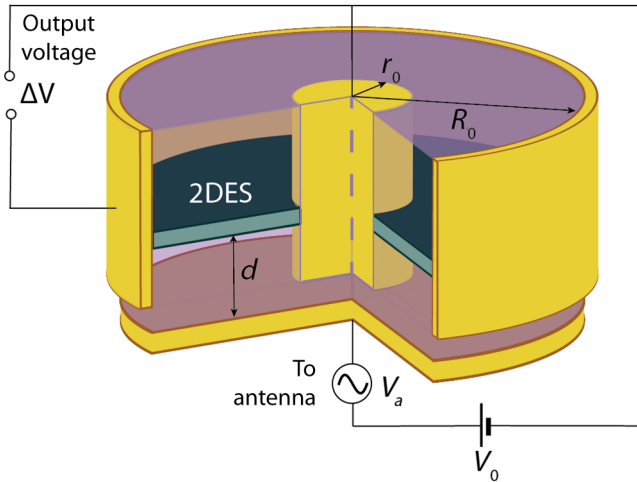


FIG. 1. Scheme of the THz detector based on 2DES in a Corbino geometry: THz radiation from the antenna creates an electric potential,  $V_a$ , between source and gate; dc photovoltage,  $\Delta V$ , due to transistor nonlinearities is read out between source and drain.

and the continuity equation for the sheet density  $n_s$ ,

$$\frac{\partial n_s}{\partial t} + \frac{1}{r} \frac{\partial}{\partial r}(r u n_s) = 0. \quad (3)$$

Here  $e$  is the electron charge,  $m$  is the electron effective mass,  $\tau_p$  is the momentum relaxation time, and  $\varphi$  is the local electric potential in the 2DES. The set of transport equations should be supplemented by Poisson's equation relating the electric potential  $\varphi$  and sheet carrier density  $n_s$ ,

$$\varphi(r) = \varphi_{\text{ext}}(r) - e \int G(r, r') n_s(r') dr', \quad (4)$$

where  $G(r, r')$  is Green's function of the electrostatic problem and  $\varphi_{\text{ext}}(r)$  is the gate-induced potential in the absence of a 2DES.

The exact solution of set (2)–(4) is possible using the method of eigenfunction expansion, which we sketch below. Here, to obtain physically traceable results, we consider the electrostatics of a Corbino device in the local-capacitance approximation relating the carrier density  $n_s(r)$  at a given point  $r$  with the gate-to-channel voltage  $V_g - \varphi(r)$ :

$$C[V_g - \varphi(r)] = e n_s(r). \quad (5)$$

The coefficient  $C = \varepsilon/4\pi d$  is the gate-channel specific capacitance and  $\varepsilon$  is the gate dielectric constant. Relation (5) can be rigorously derived if the gate-to-channel separation  $d$  is small compared to the length of charge inhomogeneity in the 2DES (see, e.g., Ref. [23]). Under these conditions, Green's function decays rapidly owing to gate screening, and can be approximated by a delta function with proper prefactor.

The set of transport equations (2)–(5) is supplemented by the following boundary conditions, respectively implying grounded source and zero ac current at the drain:

$$\varphi(r_0, t) = 0, \quad (6)$$

$$n_s u(R_0, t) = 0. \quad (7)$$

Importantly, the latter condition for ac current does not require a perfect voltmeter in the drain circuit. It is rather dictated by large inductance of bonding wires and their large reactive impedance at THz frequencies [24].

The linear-response ac electric potential in the channel is readily obtained from Eqs. (2)–(7):

$$\frac{V_a - \varphi_\omega(r)}{V_a} = \frac{Y_1(kR_0)J_0(kr) - Y_0(kr)J_1(kR_0)}{Y_1(kR_0)J_0(kr_0) - Y_0(kr_0)J_1(kR_0)}. \quad (8)$$

Here  $k = \omega/s\sqrt{1 + i(\omega\tau_p)^{-1}}$  is the plasmon wave vector,  $s = \sqrt{eV_0/m}$  is the plasma wave velocity, and  $J_i$  and  $Y_i$  are Bessel functions of the  $i$ th kind.

The obtained expression for linear-response electric potential can be used as a building block to evaluate various nonlinear rectification processes, e.g., owing to contacts with nonlinear  $I(V)$  characteristics [18] or photothermoelectric effects [25]. Here we shall focus on rectification mechanisms intrinsically present in the hydrodynamic model [11]. These mechanisms include the nonlinear dependence of electron fluid kinetic energy on the drift velocity (hydrodynamic nonlinearity) and resistive self-mixing. Their contributions to rectified voltage are denoted as  $\Delta V_{\text{hd}}$  and  $\Delta V_{\text{rsm}}$ , respectively:

$$\Delta V = \Delta V_{\text{hd}} + \Delta V_{\text{rsm}}. \quad (9)$$

Their partial contributions are given by (for derivations, see [11,26] and Appendix A)

$$\Delta V_{\text{hd}} = \frac{e|E_\omega|^2}{4m(\omega^2 + \tau_p^{-2})}, \quad (10)$$

$$\Delta V_{\text{rsm}} = \frac{1}{2V_0} \int_{r_0}^{R_0} \text{Re} \left( \frac{E_\omega U_\omega^*}{1 - i\omega\tau_p} \right) dr, \quad (11)$$

where  $E_\omega(r) = -\partial\varphi_\omega/\partial r$  is the longitudinal electric field in the channel and  $U_\omega = V_a - \varphi_\omega$  is the local gate-to-channel voltage.

### III. RESULTS: SINGULARITY-ENHANCED THz DETECTION

Once the plasmon quality factor is large,  $Q = \omega\tau_p \gg 1$ , the rectified voltage is dominated by hydrodynamic nonlinearity,  $\Delta V_{\text{hd}}/\Delta V_{\text{rsm}} \sim Q^2$ . Indeed, the hydrodynamic nonlinearity  $\Delta V_{\text{hd}}$  is proportional to the amplitude of the electron velocity that, in turn, is enhanced for higher mobility. The resistive self-mixing, on the contrary, requires large ohmic resistance of the sample and is not enhanced by plasmonic effects. Numerical comparison of these contributions to rectified voltage is presented in Fig. 2 and confirms these arguments. These facts enable us to consider only the hydrodynamic contribution to rectified voltage in high-quality samples.

As the radius of the inner contact becomes smaller, the ac electric field in its vicinity is enhanced according to  $E_\omega \approx (V_a/r_0) \ln^{-1}(e^\gamma k r_0/2)$ , where  $\gamma \approx 1.7$  is Euler's constant (see Appendix B for a derivation). Up to a logarithmic factor, this scaling coincides with the field of a charged wire that mimics a central contact.

A geometrically enhanced ac electric field near the inner contact leads to even higher ac velocity of electrons  $u_\omega$  and further enhancement of hydrodynamic nonlinearity. This result is readily seen from the comparison of responsivity spectra at various ratios  $r_0/R_0$  given in Fig. 2. The geometric enhancement is most pronounced for the

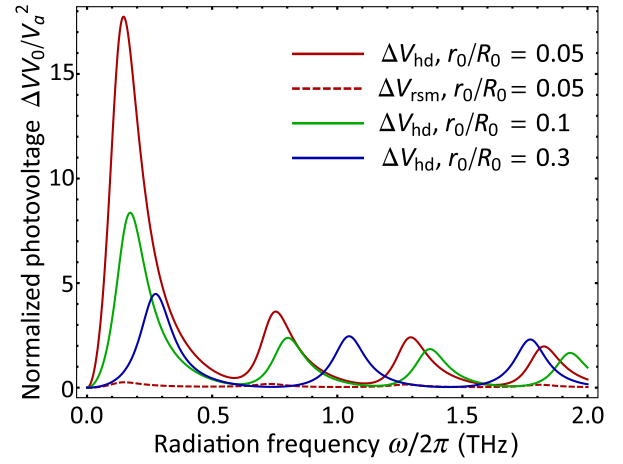


FIG. 2. Normalised response of a Corbino detector versus the radiation frequency for different inner contact dimensions,  $r_0/R_0$ . Contributions of hydrodynamic nonlinearity,  $\Delta V_{\text{hd}}$ , and resistive self-mixing,  $\Delta V_{\text{rsm}}$ , are shown with solid and dashed lines, respectively. 2DES parameters are  $s = 10^6$  m/s,  $\tau_p = 1$  ps,  $R_0 = 1$   $\mu\text{m}$ .

lowest-frequency resonant modes; it is possible to show that the rectified voltage at the first resonance is roughly  $(R_0/r_0)^2$  times greater than the next one.

It is possible to convert the rectified voltage into a practical figure of detector merit, the responsivity  $R_V = \Delta V/P$ , where  $P$  is the incident electromagnetic power. The latter is related to the ac voltage between source and drain via the antenna radiative resistance  $Z_a: P = V_a^2/2Z_a$ . Using a typical value for dipole antennas  $Z_a \approx 100$   $\Omega$ , we predict the resonant responsivity of the Corbino detector  $R_V \approx 50$  kV/W for a frequency of 0.1 THz and a momentum relaxation time  $\tau_p \approx 2$  ps. This value of responsivity exceeds that of commercially available diodes by an order of magnitude [27].

The growing rectification capability of the Corbino device with decreasing inner radius should have physical upper limits. When the contact radius  $r_0$  becomes comparable with the gate-to-channel separation  $d$ , the local-capacitance approximation becomes, strictly speaking, inapplicable. Still, it is possible to construct an exact solution for Corbino-device electrostatics and show that the local-capacitance model works fine for  $r_0 < d$  and that the growth of responsivity with decreasing  $r_0$  persists for  $r_0 < d$ .

The *exact solution* for driven electrical oscillations in a Corbino geometry is based on the expansion of the electric potential  $\varphi(r, z)$  in basis functions  $\Phi_n(r, z)$  satisfying zero boundary conditions at the contacts [24]. The expansion is supplemented by “contact contributions”  $V_d f_d(r, z)$  and  $V_g f_g(r, z)$ , representing electric potential due to the gate and drain in the absence of a 2DES. The dimensionless functions  $f_d$  and  $f_g$  satisfy unity boundary conditions at the contacts; labelling the symmetry axis of the system

as  $z$ , setting its origin in the plane of the 2DES and taking the global gate coordinate to be  $z = d$ , these conditions read  $f_d(R_0, z) = 1$  and  $f_g(r, d) = 1$ . The full expansion of potential reads

$$\varphi(r, z) = \sum_{n=1}^{\infty} c_n \Phi_n(r, z) + V_d f_d(r, z) + V_g f_g(r, z). \quad (12)$$

Here the gate voltage  $V_g$  is fixed by the antenna, the coefficients  $c_n$  (strengths of the  $n$ th plasmon modes) are found by the projection technique, and the drain voltage  $V_d$  is obtained from the zero-current boundary condition.

Explicit expressions for eigenfunctions  $\Phi_n(r, z)$  can be obtained if source and drain contacts are extended to infinity in the  $z$  direction. Physically, their height should much exceed the plasmon wavelength. In this model case, these functions are factorized:

$$\Phi_n(x, z) = v_n(r) \psi_n(z), \quad (13)$$

$$\psi_n(z) = e^{-|\Lambda_n z|} - e^{-|\Lambda_n (2d-z)|}, \quad (14)$$

$$v_n(r) = J_0(\Lambda_n r) - \frac{J_1(\Lambda_n R_0)}{Y_1(\Lambda_n R_0)} Y_0(\Lambda_n r). \quad (15)$$

The eigenvalues  $\Lambda_n$  are found from the zero boundary conditions  $v_n(r_0) = v_n(R_0) = 0$ . Once the eigenfunctions are known, we readily obtain Green's function for the electrostatic problem and particular solutions  $f_d$  and  $f_g$  (see Appendix C).

The comparison of responsivities obtained with exact and approximate electrostatic models is shown in Fig. 3. We readily observe that the local capacitance model works fine even for relatively small inner radius  $r_0 = 10$  nm comparable to the gate-channel separation  $d = 50$  nm.

#### IV. DISCUSSION AND POSSIBLE EXPERIMENTAL REALIZATION

We now discuss the physical limitations of our model. The particular value of external responsivity depends on coupling between the antenna and 2DES; the assumed relation between the incident power and gate-drain voltage  $V_a^2 = 2PZ_a$  is valid if the antenna acts as a perfect voltage source. Physically, it is valid if the antenna impedance is less than the input impedance of the transmission line formed by the gate plate and kinetic inductance [10,28]. To show the likelihood of the proposed detector being independent of coupling details, we compare the responsivity of the Corbino detector and the original proposal of Ref. [11] (“rectangular” FET with parallel source and drain contacts) calculated under identical conditions (see Fig. 4). We readily observe that the responsivity of the Corbino device

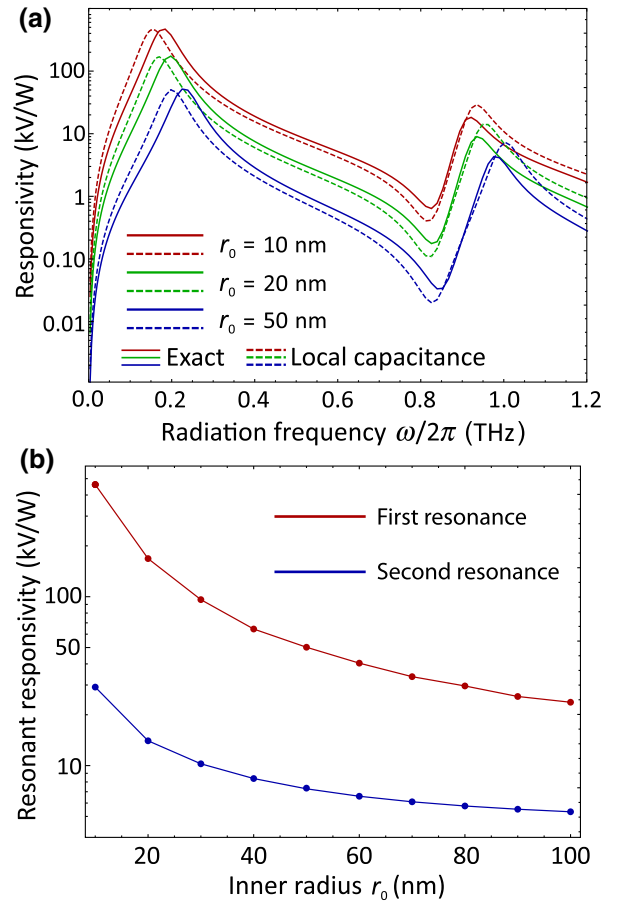


FIG. 3. (a) Calculated Corbino detector responsivity versus the radiation frequency for approximate (solid line) and exact (dashed line) solutions of the electric potential at different radii of the inner contact,  $r_0$ . (b) Responsivity at first and second harmonics of plasmon resonance versus the inner radius  $r_0$ . Here the carrier density  $n_s = 10^{12} \text{ cm}^{-2}$ , dielectric constant  $\epsilon = 12.9$  (corresponding to a plasmon velocity  $s = 1.4 \times 10^6 \text{ m/s}$ ), momentum relaxation time  $\tau_p = 2.3 \text{ ps}$ ,  $R_0 = 1 \mu\text{m}$ , gate-to-channel separation  $d = 50 \text{ nm}$ , antenna resistance  $Z_a = 100 \Omega$ , and effective mass  $m = 0.067m_0$ . The parameters correspond to the plasma wave velocity  $s = \sqrt{n_s e^2 / mC} \approx 1.4 \times 10^6 \text{ m/s}$ .

exceeds that of the “rectangular” FET by more than an order of magnitude, especially in the vicinity of the lowest resonance. As the responsivity of the original proposal has been measured in numerous works and was shown to exceed 1 kV/W [10,29], the estimate for the Corbino device exceeding 10 kV/W looks realistic.

The enhanced responsivity of the Corbino detector should hold for other local rectification mechanisms different from hydrodynamic nonlinearity. Particularly, contacts between metal and the 2DES can display rectifying behavior either due to nonlinearity of the Schottky junction  $I(V)$  characteristic [18], or due to the photothermoelectric effect at the metal-2DES junction [25,30]. Moreover, detectors made of graphene were predicted to exhibit a stronger

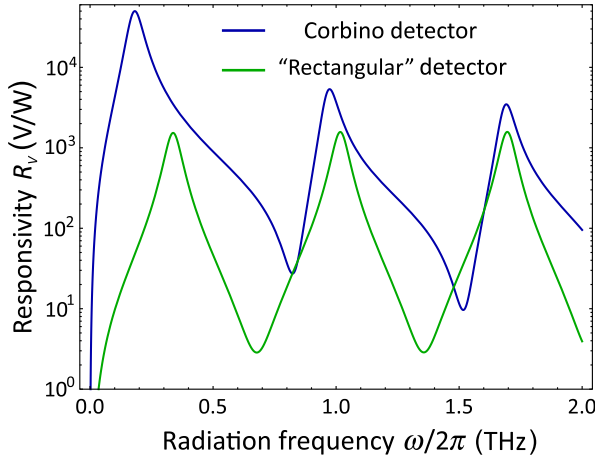


FIG. 4. Responsivities of Corbino (blue line) and “rectangular” (green line) detectors versus the radiation frequency at  $n_s = 10^{12} \text{ cm}^{-2}$ ,  $d = 50 \text{ nm}$ ,  $\varepsilon = 12.9$  (corresponding to a plasmon velocity  $s = 1.4 \times 10^6 \text{ m/s}$ ),  $\tau_p = 2.3 \text{ ps}$ ,  $r_0 = 0.03R_0$ , and antenna resistance  $Z_a = 100 \Omega$ . Source-drain separations in Corbino and “rectangular” devices are equal and taken to be  $L \equiv R_0 = 1 \mu\text{m}$ .

photoresponse owing to graphene’s linear band dispersion [31,32]. Finally, it was recently shown [33] that “hydrodynamic nonlinearity” persists in the ballistic regime as its underlying origin is the nonlinear dependence of the electron energy on velocity. Importantly, in any of these cases, the nonlinear response is approximately proportional to the squared ac electric field at the contact  $|E_\omega(r_0)|^2$ , as in the considered case of hydrodynamic nonlinearity. As the field enhancement by plasmonic and geometric effects is independent of assumed rectification physics, high responsivity of Corbino devices should hold for other rectification mechanisms. We also note that an inverse process of the dc current conversion into plasmons (plasma instability [34–36]) is also favored by large electric fields of plasmon modes at the contacts [37], and that the instability growth rate should also scale as  $r_0^{-2}$ . This remarkable scaling needs to be included in the analysis of current-driven plasmon instability in the Corbino geometry [38].

Growth of responsivity with decreasing  $r_0$  should be limited by nonlocality of rectification. The hydrodynamic nonlinearity is expected to saturate at  $r_0 \sim l_{ee}$ , where  $l_{ee}$  is the free path due to electron-electron collisions; the Schottky junction nonlinearity saturates at  $r_0 \sim l_{dep}$ , where  $l_{dep}$  is the depletion length; the photothermoelectric effect saturates at  $r_0 \sim l_T$ , where  $l_T$  is the heat diffusion length. Finally, the decrease in the inner contact radius increases the total resistance of the device  $R_{tot}$ . However, the latter scales with  $r_0$  only logarithmically,  $R_{tot} \propto \ln R_0/r_0$ , and does not have much effect on the current responsivity  $R_I = R_V/R_{tot}$  and noise-equivalent power  $NEP \propto \sqrt{R_{tot}}/R_V$ .

The current technology of 2D electron systems enables the fabrication of proposed THz detectors. Indeed, the

quality of 2D heterostructures is sufficient to observe plasmon resonances at THz and sub-THz frequencies [6,10], particularly in the Corbino geometry [39]. Plasmonic rectification of sub-THz signals in the ring geometry has also been observed [40]. In the reported detector, however, the rectifying contacts were placed along the perimeter of the 2DES, which did not allow for the geometric enhancement of the ac field to be exploited as in this work.

In summary, we have shown a strong enhancement of responsivity in THz and sub-THz detectors based on 2D electron systems in the Corbino geometry. The enhancement appears due to a combination of plasmon resonance and electric field enhancement near the central contact of small radius. We have shown that it is possible to achieve external responsivity exceeding  $10 \text{ kV/W}$  at a 200 GHz frequency for realistic sample dimensions and momentum relaxation times, if the photoresponse is governed by hydrodynamic nonlinearity. The proposed effect of combined geometric-plasmonic responsivity enhancement should be observable not only in the Corbino geometry with small central contact, but also in other structures with keen or sharp metal electrodes and can be extended to other detection mechanisms, e.g., of photothermoelectric origin.

The data that support the findings of this study are available from the corresponding author upon reasonable request.

## ACKNOWLEDGMENTS

This work was supported the Russian Scientific Foundation under Grant No. 18-72-00234. The authors thank D. Svintsov, A. Tomadin, A. Principi, V. Muraviev, W. Knap, and A. Laisuskas for helpful discussions, and Yu. Kharchenko for a designer’s perspective.

## APPENDIX A. LINEAR RESPONSE AND RECTIFIED VOLTAGE

The solution to the coupled Poisson and hydrodynamic equations is represented as a series in powers of antenna voltage  $V_a$ :

$$U(r, t) = \bar{U} + U_1 + U_2 \dots, \quad (\text{A1})$$

$$u(r, t) = \bar{u} + u_1 + u_2 \dots \quad (\text{A2})$$

Here  $\bar{u}$  and  $\bar{U}$  are the time-averaged electron velocity and gate-to-channel potential, respectively, and  $u_n$  and  $U_n$  vary with time with frequency  $n\omega$ , where  $\omega$  is the frequency of the input signal. The terms  $U_1$  and  $u_1$  are proportional to the first power of  $V_a$ . They are governed by the linearized equations

$$\frac{\partial u_1}{\partial t} + \frac{u_1}{\tau_p} + \frac{e}{m} \frac{\partial U_1}{\partial r} = 0, \quad (\text{A3})$$

$$\frac{\partial U_1}{\partial t} + \frac{V_0}{r} \frac{\partial(ru_1)}{\partial r} = 0, \quad (\text{A4})$$

where we have expressed the electron sheet density  $n_s$  via the electric potential. Searching for the solutions proportional to  $e^{-i\omega t}$ , we obtain the equations for gate-to-channel potential and velocity:

$$k^2 r^2 U_1 + rU_1' + r^2 U_1'' = 0, \quad (\text{A5})$$

$$(k^2 r^2 - 1)u_1 + ru_1' + r^2 u_1'' = 0. \quad (\text{A6})$$

Here  $k^2 = \omega^2/s^2(1 + i/\omega\tau_p)$  is the squared plasmon wave vector. The solution is a combination of Bessel functions:

$$U_1 = C_1 J_0(kr) + C_2 Y_0(kr). \quad (\text{A7})$$

The constants are determined from boundary conditions (6) and (7); we obtain a solution for the gate-to-channel potential in the form of Eq. (8).

The second order time-averaged quantities are governed by

$$\frac{\partial}{\partial r} \left( \frac{\bar{u}_1^2}{2} - \frac{e\bar{U}}{m} \right) + \frac{\bar{u}}{\tau_p} = 0, \quad (\text{A8})$$

$$\frac{\partial}{\partial r} (V_0 \bar{u}r - \bar{U}_1 u_1 r) = 0. \quad (\text{A9})$$

These equations lead to the following expressions for the rectified potential and velocity (keeping in mind that  $\bar{U} = -\bar{\varphi}$ ):

$$\bar{\varphi}(R_0) - \bar{\varphi}(r_0) = -\frac{m|u_1(r_0)|^2}{2e} + \frac{m}{e\tau_p} \int_{r_0}^{R_0} \bar{u}dr, \quad (\text{A10})$$

$$\bar{u} = \frac{\bar{U}_1 u_1}{V_0}. \quad (\text{A11})$$

The first term in (A10) corresponds to hydrodynamic nonlinearity,

$$\Delta V_{\text{hd}} = -\frac{m|u_1(r_0)|^2}{2e}, \quad (\text{A12})$$

and the second term corresponds to the resistive self-mixing effect,

$$\Delta V_{\text{rsm}} = \frac{m}{e\tau_p} \int_{r_0}^{R_0} \bar{u}dr. \quad (\text{A13})$$

To obtain Eqs. (10) and (11), it is sufficient to express the drift velocity  $u_1$  via the electric field  $\partial U_1/\partial x$ .

## APPENDIX B: ANALYTICAL ESTIMATES OF RESPONSIVITY

The hydrodynamic contribution to responsivity can be analytically maximized in the nearly collisionless regime  $\omega\tau_p \gg 1$ . If the  $k_n$  are values of the wave vector corresponding to resonance, the maximum output voltage is given by

$$\Delta V_{\text{hd}} = \frac{V_a^2 \tau_p^2 s^2}{V_0 R_0^2} \frac{D_1^2(r_0, R_0)}{(r_0 D_1(r_0, R_0)/R_0 - D_0(r_0, R_0))^2}, \quad (\text{B1})$$

where

$$D_i(r_0, R_0) = \begin{vmatrix} Y_i(k_n r_0) & J_i(k_n r_0) \\ Y_i(k_n R_0) & J_i(k_n R_0) \end{vmatrix},$$

$$i = 1, 2 \text{ and } k_n = \frac{\omega_n}{s}.$$

The above expression agrees very well with the hydrodynamic response evaluated with the full form of the electric potential, as shown in Fig. 5. We can further simplify this expression at small radii of the inner contact  $k_n r_0 \ll 1$ . Under such conditions,

$$D_1(r_0, R_0) \simeq J_1(k_n R_0) Y_1(k_n r_0) \simeq \frac{J_1(k_n R_0)}{k_n r_0}, \quad (\text{B2})$$

$$D_0(r_0, R_0) \simeq J_0(k_n R_0) Y_0(k_n r_0) \simeq J_0(k_n R_0) \ln(k_n r_0), \quad (\text{B3})$$

$$D_1(r_0, R_0) \gg D_0(r_0, R_0). \quad (\text{B4})$$

With these expansions, Eq. (B1) can be simplified as

$$\Delta V_{\text{hd}} \simeq \frac{V_a^2}{V_0} \frac{\tau_p^2 s^2}{(R_0 k_n r_0)^2 \ln(k_n r_0)^2} \frac{J_1^2(k_n R_0)}{J_0^2(k_n R_0)}. \quad (\text{B5})$$

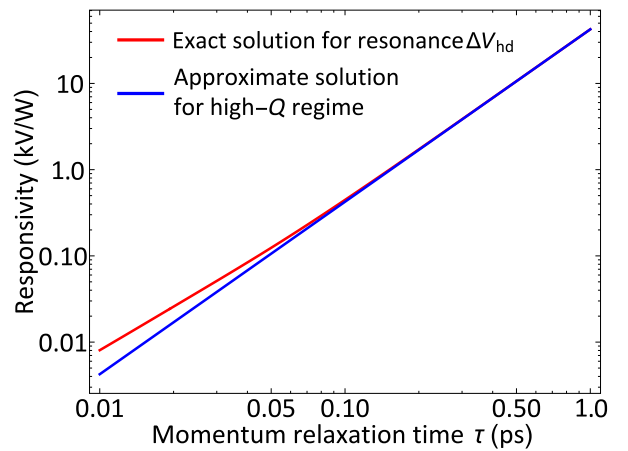


FIG. 5. Hydrodynamic responsivity at the fundamental resonance evaluated using exact [(8) and (10)] and approximate [(B1)] equations versus the momentum relaxation time  $\tau_p$ . The parameters of the system are  $s = 10^6$  m/s,  $R_0 = 1$   $\mu\text{m}$ ,  $r_0 = 30$  nm, and antenna impedance  $Z_a = 100$   $\Omega$ .

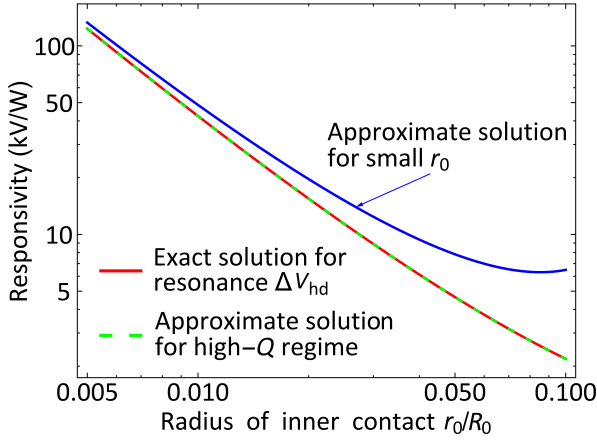


FIG. 6. Resonance responsivity of a Corbino detector using exact and approximate solutions for the high- $Q$  regime for different inner contact radii,  $r_0/R_0$ . The 2DES parameters are  $s = 10^8$  cm/s,  $R_0 = 1 \mu\text{m}$ , and  $\tau_p = 1$  ps.

The agreement of Eq. (B5) with the exact hydrodynamic response is very good at  $r_0/R_0 \lesssim 0.01$ , as shown in Fig. 6. In the opposite, over-damped mode  $\omega\tau_p \ll 1$ , the real and imaginary parts of the wave vector are equal to  $k_0 = (1/s)(\omega/\tau_p)^{1/2}$ . If the damping is strong enough that  $k_0 r_0 \gg 1$ , we can use the expansions of Bessel functions at large arguments in Eqs. (10) and (11). Both components of the rectified voltage are evaluated analytically, yielding

$$\Delta V_{\text{hd}} \simeq \frac{V_a^2}{V_0} \frac{\omega^2}{8s^2 k_0^2} f[k_0(R_0 - r_0)], \quad (\text{B6})$$

$$\Delta V_{\text{ism}} \simeq \frac{V_a^2}{V_0} \frac{\omega}{8s^2 \tau_p k_0^2} f[k_0(R_0 - r_0)], \quad (\text{B7})$$

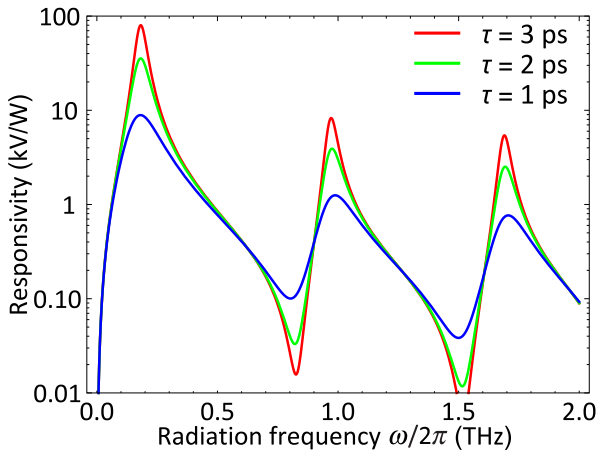


FIG. 7. Normalised response of a Corbino detector for different momentum relaxation times  $\tau_p$ . The 2DES parameters are  $s = 10^8$  cm/s,  $R_0 = 1 \mu\text{m}$ , and  $r_0 = 0.03 \mu\text{m}$ .

where  $f(x)$  is the dimensionless function

$$f(x) = \frac{\sin^2 2x + \sinh^2 2x}{(\cos 2x + \cosh 2x)^2}. \quad (\text{B8})$$

The transition from the highly-resonant to nonresonant regime is illustrated in Fig. 7.

### APPENDIX C: EXACT SOLUTION FOR DRIVEN OSCILLATIONS IN THE CORBINO GEOMETRY

The central object to find the electric potential due to the gate and drain in the absence of a 2DES is Green's function of the electrostatic problem. Once the eigenmodes of the Laplace operator in the Corbino geometry  $\Phi_n(r, z)$  are known, Green's function is expressed as

$$G(r, r', z, z') = \frac{1}{4\pi} \sum_{n=1}^{\infty} \frac{v_n(r')v_n(r)}{\Lambda_n} (e^{-\Lambda_n|z-z'|} - e^{-\Lambda_n|z+z'-2d|}), \quad (\text{C1})$$

where

$$v_n(r) = J_0(\Lambda_n r) - \frac{J_1(\Lambda_n R_0)}{Y_1(\Lambda_n R_0)} Y_0(\Lambda_n r), \quad (\text{C2})$$

and the  $\Lambda_n$  are found from the condition  $v_n(r_0) = 0$ . We do not consider the modes with angle-dependent electric potential proportional to  $e^{im\theta}$ , as they do not couple to radially symmetric field.

The functions  $f_d(r, z)$  and  $f_g(r, z)$  in Eq. (10) are electric potentials created in all space when the potential of the drain (gate) is set to unity. These can both be found using the fundamental solution of the Laplace equation:

$$f_d(r, z) = -R_0 \sum_{n=1}^{\infty} \frac{v'_n(R_0)v_n(r)}{\Lambda_n^2} (1 - e^{-\Lambda_n(d-z)}), \quad (\text{C3})$$

$$f_g(r, z) = \sum_{n=1}^{\infty} v_n(r) e^{-\Lambda_n(d-z)} \int_{r_0}^{R_0} v_n(r') r' dr'. \quad (\text{C4})$$

Here  $v'_n(r)$  denotes the derivative of  $v_n(r)$ .

- 
- [1] Saba Siadat Mousavi, Andreas Stöhr, and Pierre Berini, Plasmonic photodetector with terahertz electrical bandwidth, *Appl. Phys. Lett.* **104**, 143112 (2014).  
 [2] Wei Wu, Alireza Bonakdar, and Hooman Mohseni, Plasmonic enhanced quantum well infrared photodetector with high detectivity, *Appl. Phys. Lett.* **96**, 161107 (2010).

- [3] Fang-Fang Ren, Kah-Wee Ang, Junfeng Song, Qing Fang, Mingbin Yu, Guo-Qiang Lo, and Dim-Lee Kwong, Surface plasmon enhanced responsivity in a waveguided germanium metal-semiconductor-metal photodetector, *Appl. Phys. Lett.* **97**, 091102 (2010).
- [4] D. M. Schaadt, B. Feng, and E. T. Yu, Enhanced semiconductor optical absorption via surface plasmon excitation in metal nanoparticles, *Appl. Phys. Lett.* **86**, 063106 (2005).
- [5] A. El Fatimy, F. Teppe, N. Dyakonova, W. Knap, D. Seluta, G. Valušis, A. Shchepetov, Y. Roelens, S. Bollaert, A. Cappy, and S. Rumyantsev, Resonant and voltage-tunable terahertz detection in InGaAs/InP nanometer transistors, *Appl. Phys. Lett.* **89**, 131926 (2006).
- [6] P. S. Dorozhkin, S. V. Tovstonog, S. A. Mikhailov, I. V. Kukushkin, J. H. Smet, and K. von Klitzing, Resonant detection of microwave radiation in a circular two-dimensional electron system with quantum point contacts, *Appl. Phys. Lett.* **87**, 092107 (2005).
- [7] X. G. Peralta, S. J. Allen, M. C. Wanke, N. E. Harff, J. A. Simmons, M. P. Lilly, J. L. Reno, P. J. Burke, and J. P. Eisenstein, Terahertz photoconductivity and plasmon modes in double-quantum-well field-effect transistors, *Appl. Phys. Lett.* **81**, 1627 (2002).
- [8] P. A. Gusikhin, V. M. Muravev, A. A. Zagitova, and I. V. Kukushkin, Drastic Reduction of Plasmon Damping in Two-Dimensional Electron Disks, *Phys. Rev. Lett.* **121**, 176804 (2018).
- [9] Pablo Alonso-González, Alexey Y. Nikitin, Yuanda Gao, Achim Woessner, Mark B. Lundberg, Alessandro Principi, Nicolò Forcellini, Wenjing Yan, Saül Vélez, Andreas J. Huber, Kenji Watanabe, Takashi Taniguchi, Félix Casanova, Luis E. Hueso, Marco Polini, James Hone, Frank H. L. Koppens, and Rainer Hillenbrand, Acoustic terahertz graphene plasmons revealed by photocurrent nanoscopy, *Nat. Nanotechnol.* **12**, 31 (2017).
- [10] Denis A. Bandurin, Dmitry Svintsov, Igor Gayduchenko, Shuigang G. Xu, Alessandro Principi, Maxim Moskotin, Ivan Tretyakov, Denis Yagodkin, Sergey Zhukov, Takashi Taniguchi, K. Watanabe, I. V. Grigorieva, M. Polini, G. Goltsman, A. K. Geim, and G. Fedorov, Resonant terahertz detection using graphene plasmons, *Nat. Commun.* **9**, 5392 (2018).
- [11] M. Dyakonov and M. Shur, Detection, mixing, and frequency multiplication of terahertz radiation by two-dimensional electronic fluid, *IEEE Trans. Electron Devices* **43**, 380 (1996).
- [12] Valeria Giliberti, Alessandra Di Gaspare, Ennio Giovine, Michele Ortolani, Lucia Sorba, Giorgio Biasiol, Vyacheslav V. Popov, Denis V. Fateev, and Florestano Evangelisti, Downconversion of terahertz radiation due to intrinsic hydrodynamic nonlinearity of a two-dimensional electron plasma, *Phys. Rev. B* **91**, 165313 (2015).
- [13] Wojciech Knap, Mikhail Dyakonov, Dominique Coquillat, Frederic Teppe, Nina Dyakonova, Jerzy Łusakowski, Krzysztof Karpierz, Maciej Sakowicz, Gintaras Valušis, Dalius Seluta, Irmantas Kasalynas, Abdelouahad El Fatimy, Y. M. Meziani, and Taiichi Otsuji, Field effect transistors for terahertz detection: Physics and first imaging applications, *J. Infrared Millimeter Terahertz Waves* **30**, 1319 (2009).
- [14] Audrey Zak, Michael A. Andersson, Maris Bauer, Jonas Matukas, Alvydas Lisauskas, Hartmut G. Roskos, and Jan Stake, Antenna-integrated 0.6 THz fet direct detectors based on CVD graphene, *Nano Lett.* **14**, 5834 (2014).
- [15] L. Vicarelli, M. S. Vitiello, D. Coquillat, Antonio Lombardo, Andrea Carlo Ferrari, W. Knap, M. Polini, V. Pellegrini, and Alessandro Tredicucci, Graphene field-effect transistors as room-temperature terahertz detectors, *Nat. Mater.* **11**, 865 (2012).
- [16] J. B. Pendry, Paloma Arroyo Huidobro, Yu Luo, and Emanuele Galiffi, Compacted dimensions and singular plasmonic surfaces, *Science* **358**, 915 (2017).
- [17] Chih-Wei Chuang, Connie Chang-Hasnain, Forrest Grant Sedgwick, and Wai Son Ko, Nanoneedle plasmonic photodetectors and solar cells, U.S. Patent No. US8,809,672 (2014).
- [18] Victor Ryzhii and Michael S. Shur, Resonant terahertz detector utilizing plasma oscillations in two-dimensional electron system with lateral Schottky junction, *Jpn. J. Appl. Phys.* **45**, L1118 (2006).
- [19] V. M. Muravev and I. V. Kukushkin, Plasmonic detector/spectrometer of subterahertz radiation based on two-dimensional electron system with embedded defect, *Appl. Phys. Lett.* **100**, 082102 (2012).
- [20] Andrew Lucas and Kin Chung Fong, Hydrodynamics of electrons in graphene, *J. Phys.: Condens. Matter* **30**, 053001 (2018).
- [21] Denis A. Bandurin, Andrey V. Shytov, Leonid S. Levitov, Roshan Krishna Kumar, Alexey I. Berdyugin, Moshe Ben Shalom, Irina V. Grigorieva, Andre K. Geim, and Gregory Falkovich, Fluidity onset in graphene, *Nat. Commun.* **9**, 1 (2018).
- [22] Joseph A. Sulpizio, Lior Ella, Asaf Rozen, John Birkbeck, David J. Perello, Debarghya Dutta, Moshe Ben-Shalom, Takashi Taniguchi, Kenji Watanabe, Tobias Holder, Raquel Queiroz, Alessandro Principi, Ady Stern, Thomas Scaffidi, Andre K. Geim, and Shahal Ilani, Visualizing poiseuille flow of hydrodynamic electrons, *Nature* **576**, 75 (2019).
- [23] A. O. Govorov, V. M. Kovalev, and A. V. Chaplik, Solitons in semiconductor microstructures with a two-dimensional electron gas, *JETP Lett.* **70**, 488 (1999).
- [24] D. Svintsov, Exact Solution for Driven Oscillations in Plasmonic Field-Effect Transistors, *Phys. Rev. Appl.* **10**, 024037 (2018).
- [25] D. A. Bandurin, I. Gayduchenko, Y. Cao, M. Moskotin, A. Principi, I. V. Grigorieva, G. Goltsman, G. Fedorov, and D. Svintsov, Dual origin of room temperature sub-terahertz photoresponse in graphene field effect transistors, *Appl. Phys. Lett.* **112**, 141101 (2018).
- [26] M. Sakowicz, M. B. Lifshits, O. A. Klimenko, F. Schuster, D. Coquillat, F. Teppe, and W. Knap, Terahertz responsivity of field effect transistors versus their static channel conductivity and loading effects, *J. Appl. Phys.* **110**, 054512 (2011).
- [27] <https://terasense.com/products/detectors/>.
- [28] Gregory R. Aizin and Gregory C. Dyer, Transmission line theory of collective plasma excitations in periodic two-dimensional electron systems: Finite plasmonic crystals and tamm states, *Phys. Rev. B* **86**, 235316 (2012).
- [29] Alvydas Lisauskas, Maris Bauer, Sebastian Boppel, Martin Mundt, Bassam Khamaisi, Eran Socher, Rimvydas



- Venckevičius, Linas Minkevičius, Irmantas Kašalynas, Dalius Seliuta, Gintaras Valušis, Viktor Krozer, and Hartmut G. Roskos, Exploration of terahertz imaging with silicon mosfets, *J. Infrared Millimeter Terahertz Waves* **35**, 63 (2014).
- [30] Sebastián Castilla, Bernat Terrés, Marta Autore, Leonardo Viti, Jian Li, Alexey Y. Nikitin, Ioannis Vangelidis, Kenji Watanabe, Takashi Taniguchi, Eleftherios Lidorikis, Miriam S. Vitiello, Rainer Hillenbrand, Klaas-Jan Tielrooij, and Frank H. L. Koppens, Fast and sensitive terahertz detection using an antenna-integrated graphene pn junction, *Nano Lett.* **19**, 2765 (2019).
- [31] Andrea Tomadin and Marco Polini, Theory of the plasma-wave photoresponse of a gated graphene sheet, *Phys. Rev. B* **88**, 205426 (2013).
- [32] Andrea Tomadin, Alessandro Tredicucci, Vittorio Pellegrini, Miriam S. Vitiello, and Marco Polini, Photocurrent-based detection of terahertz radiation in graphene, *Appl. Phys. Lett.* **103**, 211120 (2013).
- [33] Alessandro Principi, Denis Bandurin, Habib Rostami, and Marco Polini, Pseudo-euler equations from nonlinear optics: Plasmon-assisted photodetection beyond hydrodynamics, *Phys. Rev. B* **99**, 075410 (2019).
- [34] Michael Dyakonov and Michael Shur, Shallow Water Analogy for a Ballistic Field Effect Transistor: New Mechanism of Plasma Wave Generation by dc Current, *Phys. Rev. Lett.* **71**, 2465 (1993).
- [35] Christian B. Mendl and Andrew Lucas, Dyakonov-shur instability across the ballistic-to-hydrodynamic crossover, *Appl. Phys. Lett.* **112**, 124101 (2018).
- [36] Christian B. Mendl, Marco Polini, and Andrew Lucas, Coherent terahertz radiation from a nonlinear oscillator of viscous electrons, arXiv:1909.11093 [cond-mat.mes-hall] (2019).
- [37] Aleksandr S. Petrov and Dmitry Svintsov, Perturbation theory for two-dimensional hydrodynamic plasmons, *Phys. Rev. B* **99**, 195437 (2019).
- [38] O. Sydoruk, R. R. A. Syms, and L. Solymar, Plasma oscillations and terahertz instability in field-effect transistors with corbino geometry, *Appl. Phys. Lett.* **97**, 263504 (2010).
- [39] V. M. Muravev, A. M. Zarezin, P. A. Gusikhin, A. V. Shupletsov, and I. V. Kukushkin, Proximity plasma excitations in disk and ring geometries, *Phys. Rev. B* **100**, 205405 (2019).
- [40] P. S. Dorozhkin, S. V. Tovstonog, S. A. Mikhailov, I. V. Kukushkin, J. H. Smet, and K. von Klitzing, Resonant detection of microwave radiation in a circular two-dimensional electron system with quantum point contacts, *Appl. Phys. Lett.* **87**, 092107 (2005).